RSC Advances

PAPER

View Article Online
View Journal | View Issue

Cite this: *RSC Adv.*, 2025, **15**, 39417

Research on the migration and transformation patterns of volatile pyrolysis products of WPCB by an online pyrolysis-mass spectrometry method

Meng Tian, [a] Zihe Liu,[a] Dongyin Ren, [b] Xianglan Zhang*[a] and Cai Tie*[a]

Understanding the release patterns of brominated and chlorinated flame retardants during the pyrolysis of different types of wasted printed circuit boards (WPCB) is of crucial significance for the resource utilization of WPCB. The non-metallic parts of copper-clad laminates with wood pulp paper as the substrate (PL-NWCCL) and the non-metallic parts of waste printed circuit boards with glass fiber as the substrate (FR4-NWPCB) were chosen as materials. Proximate analysis, elemental analysis, ion chromatography for oxygen and nitrogen, thermogravimetric analysis (TG), and Fourier-transform infrared spectroscopy (FTIR) were employed to analyze their composition, halogen content, pyrolysis characteristics, and functional groups. An on-line pyrolysis-mass spectrometry (Py-MS) system was designed to conduct dynamic and real-time monitoring of the pyrolysis volatile products of the two materials throughout the process, aiming to systematically explore the migration and transformation patterns of volatile product components during the pyrolysis of WPCBs. Online pyrolysis-mass spectrometry analysis reveals that during the pyrolysis of the two materials, the migration and transformation patterns of Br and Cl are different. In PL-WCCL, the cellulose induces a "delaying" effect on the release of Br and Cl. There are two distinct release phases within the primary weight-loss temperature ranges of 233–330 °C and 470–530 °C. In contrast, for FR4-WPCB, the release of Br and Cl remains unaffected by the substrate and is essentially complete within the primary weight-loss temperature range of 292–422 °C. By setting different isothermal holding periods during the pyrolysis process, the sequential release order of pyrolysis products can be ascertained. This further suggests that Cl· and Br· tend to bind preferentially with hydrocarbon radicals first and subsequently with H· radicals.

Received 7th September 2025
Accepted 11th October 2025

DOI: 10.1039/d5ra06737e

rsc.li/rsc-advances

1 Introduction

Printed circuit boards (PCB) consist[1–3] of metals, resins, flame retardants, substrates, and curing agents.[4] Among them, the major types of substrates are glass fiber[5] and wood pulp paper,[6] and the primary types of flame retardants are brominated flame retardants[7] and chlorinated flame retardants.[8] It is projected that the annual global generation of waste printed circuit boards (WPCB) will reach 4.92 million tons by 2030.[9,10] WPCB contain a high proportion of metals and are a crucial component of "urban mines".[11] Nevertheless, the non-metallic fractions of waste printed circuit boards (NWPCB) are hardly biodegradable in the natural environment, resulting in substantial accumulation. Of particular concern is that the halogenated flame retardants[12] contained therein, if not properly treated, may lead to the release of environmental pollutants and pose risks to human health.[13] Consequently, the recycling and utilization of WPCB encounter the dual challenges of "resource recovery and environmental pollution".[14]

Pyrolysis, as the most versatile and robust recycling technology for waste printed circuit boards (WPCB) to date, has the ability to transform WPCB into high-value-added materials.[15] Consequently, pyrolysis is currently the mainstream strategy for "upcycling".[16] The pyrolysis enables the effective recovery of non-metallic substances from the non-metallic fraction of waste printed circuit boards (NWPCB), which can be further converted into a variety of fuels, valuable chemicals, and other materials.[17] The economic analysis of an electronic waste pyrolysis plant with an annual processing capacity of 2000 tons reveals that the expected annual rate of return is 20%, the investment payback period is 6 years, and the profitability index is 1.25.[18]

WPCB with glass fiber as substrates is dominant, and because the chemical properties of its main component SiO_2 are stable, regardless of whether microwave pyrolysis[19] or conventional pyrolysis[20] is employed, its properties remain unaltered, facilitating secondary utilization after recovery. Current research predominantly focuses on selecting diverse energy sources such as traditional electrical heating,[21] microwave pyrolysis,[22] and infrared pyrolysis,[23] *etc.*, controlling various

[a]*School of Chemical and Environmental Engineering, China University of Mining and Technology (Beijing), Beijing 100083, PR China. E-mail: zhxl@cumtb.edu.cn; tiecai@cumtb.edu.cn; Tel: +86-135-2170-3609*

[b]*College of Textile and Clothing, Dezhou University, Dezhou 253023, PR China*

pyrolysis atmospheres such as a vacuum atmosphere or an inert atmosphere, adjusting the heating rates and pyrolysis temperatures[24] to modulate the pyrolysis products and the generation ratios of solid, liquid, and gas-phase products. W. Chen[25] characterized the solid, liquid, and gas-phase products generated from the pyrolysis of the non-metallic fraction of glass-fiber-based WPCB (also known as FR4-WPCB) under different experiment conditions. The study revealed that during pyrolysis at 550 °C, the main liquid-phase products were phenol and alkylated phenols, while the main gas-phase products were CO_2, CH_4, and H_2.

The principal research regarding the migration and removal mechanisms of brominated flame retardants during the pyrolysis of FR4-WPCB is concisely presented below. Z. Yao[11] carried out an in-depth investigation and a comprehensive summary of the transformation of Br during the pyrolysis of WPCB. The findings of this study indicated that over 60wt% of the Br in the non-metallic fraction of WPCBs was transferred to the gaseous phase, while 36 wt% was retained within the solid and liquid-phase products. Moreover, an increase in the pyrolysis temperature led to a higher proportion of Br being transferred to the gaseous-phase products. Y. Wu[26] utilized *in situ* Py-TOF-MS in conjunction with Py-GC/MS techniques to explore the migration and transformation patterns of Br in copper-free WPCBs. The research demonstrated that Br was predominantly present in the liquid and gaseous-phase products in the forms of organic bromides (such as bromophenols and bromoalkanes) and HBr/Br_2. J. Liu[27] employed TG-FTIR-MS technology to study the behavior of Br in the absence of Fe during the pyrolysis of WPCBs. It was found that Br mainly existed in the form of organic bromides, resulting in the formation of compounds such as C_6H_5BrO, CH_3Br, and C_6H_5Br. J. Xiong[28] conducted TG-FTIR-GC/MS analyses and determined that brominated derivatives were formed during the pyrolysis of WPCBs. The detected products included HBr, CH_3Br, C_2H_5Br, C_3H_5Br, C_3H_7Br, $C_6H_4Br_2O$, and C_6H_5BrO. Evidently, during the pyrolysis process, certain ether bonds were initially cleaved, yielding bisphenol A, propanol, and tetrabromobisphenol A. Subsequently, tetrabromobisphenol A decomposed into C_6H_5BrO and HBr, and these two decomposition products further reacted with small molecules to generate brominated derivatives. Notably, to date, there has been a paucity of research on the detection, migration, and removal mechanisms of chlorinated flame retardants in FR4-WPCBs during its pyrolysis process.

In recent years, research on the pyrolysis of waste printed circuit boards with wood-pulp paper as the substrate or paper laminated waste copper-clad laminates has witnessed an increase. These researches primarily focus on aspects such as the distribution of three-phase products during pyrolysis under vacuum conditions,[29] kinetic analysis of pyrolysis under non-isothermal conditions,[30,31] and the removal pattern of Br during the pyrolysis process.[1,32] G. Grause[6] employed thermogravimetry (TG), thermogravimetry-mass spectrometry (TG-MS), and gas chromatography-mass spectrometry (GC-MS) to investigate and detect the pyrolysis products of tetrabromobisphenol A (TBBPA) in paper laminated waste copper-clad laminates (PL-WCCL). It was found that brominated aromatic compounds were formed in the temperature range of 270–450 °C. In contrast, pure TBBPA did not yield such products under the same experimental conditions. M. Haghi[1,32] conducted co-pyrolysis experiments on calcium oxide (CaO), calcium hydroxide ($Ca(OH)_2$), and the non-metallic fraction of PL-WCCLs. Hydrochloric acid (HCl) and hydrogen bromide (HBr) were detected in the liquid and gas-phase products. Notably, when the addition ratio (FR2-PCB-to-additive ratio) was 5.4 : 1, over 91% of Br was immobilized in the solid-phase products. Nevertheless, in this study, the removal pattern of Cl was not further analyzed. Cellulose is the main component of wood-pulp paper. A study on the co-pyrolysis of cellulose and chlorine-containing substances indicated that cellulose decomposes in the temperature range of 315–500 °C,[33] which exerts an inhibitory effect on the removal of Cl,[34] thereby significantly reducing the dechlorination efficiency.[35] However, to date, no research has explored the influence of wood-pulp paper as the substrate on the migration and transformation of halogens during the pyrolysis of PL-WCCL.

In light of the above, existing related studies predominantly utilize combined thermo-analytical and mass spectrometric techniques, such as TG-MS,[36] TG-FTIR,[37] TG-FTIR-MS,[27] py-GC/MS[38] and Py-TOF-MS,[26] to analyze the decomposition behavior patterns, product compositions, and pyrolysis reaction mechanisms of waste printed circuit boards (WPCB) during the pyrolysis process. At present, research on FR4-WPCB is mainly concentrated on brominated flame retardants, and the related investigations are relatively extensive.[39] However, the release mechanisms of halogenated flame retardants in PL-WCCL during pyrolysis still await further in-depth exploration. Particularly, when both chlorinated and brominated flame retardants are present simultaneously, there have been no published reports on the release mechanisms and their differences of Cl and Br in WPCB with different substrates during the pyrolysis process.

Current studies on the migration patterns of pyrolysis products of chlorinated flame retardants during the pyrolysis of WPCB remain insufficient. Furthermore, there is still no definitive conclusion regarding the reaction mechanisms when both chlorinated and brominated flame retardants are present simultaneously during the pyrolysis of WPCB with different substrates (fiberglass FR4 or pulp paper PL). Consequently, in this study, two types of WPCB were employed as experiment materials, which are the non-metallic fractions of copper-clad laminates with wood-pulp paper as the substrate (PL-NWCCL) and the non-metallic fractions of waste printed circuit boards with glass fiber as the substrate (FR4-NWPCB). An in-house designed on-line pyrolysis-mass spectrometry (Py-MS) coupling apparatus was utilized to perform a comprehensive, dynamic monitoring of the entire WPCB pyrolysis process. The types of volatile products generated during the pyrolysis of the non-metallic components of WPCBs with different substrates were systematically analyzed and identified. Particular emphasis was placed on elucidating the formation mechanisms of volatile derivatives of brominated and chlorinated flame retardants during pyrolysis. This study establishes a foundation

for optimizing the selection of dehalogenation agents during the pyrolysis of WPCB and the further improvement of dehalogenation efficiency. Moreover, this paper also offers a theoretical framework and technical support for the sustainable management of brominated waste materials.

2 Materials and methods

2.1 Raw materials

In this study, the raw materials employed were two types of waste printed circuit boards (WPCBs) produced by Guangdong Jiantao Chemical Co., Ltd. One was paper laminated wasted copper clad laminate (hereinafter referred to as PL-WCCL) with wood pulp paper as the substrate. After manually stripping the copper foil, the non-metallic component of PL-WCCL was abbreviated to PL-NWCCL. The other was an FR4-type waste printed circuit board (hereinafter referred to as FR4-WPCB) with glass fiber as the substrate. The non-metallic powder obtained after crushing and separating the metal substances was abbreviated to FR4-NWPCB.

2.2 Characterization of raw materials

The surface morphological characteristics of the two raw materials were examined with an electron scanning microscope (TESCAN MIRA LMS). The test conditions were as follows: acceleration voltage of 15 kV, beam current intensity at low level, energy – dispersive X-ray spectroscopy (EDS) line and surface scanning, and back-scattered electron (BSE) probe mode. The proximate analysis of the raw materials was carried out in accordance with "Proximate Analysis of Coal" (GB/T 212-2008). The tests were conducted using a GW-300c box-type resistance furnace (Coal Quality Instrument Research Center, China Coal Research Institute, China). An elemental analyzer (Vario MACRO cube, Germany) was employed for the major element analysis. Regarding the determination of trace elements and halogen content, three samples of each raw material were selected. According to the standard for halogen determination in thermoplastic elastomers (GB/T 34692-2017 "oxygen bomb combustion-ion chromatography method"), an oxygen bomb calorimeter (Model SHR-15, Nanjing Sangli Electronic Equipment Factory) and an ion chromatograph (CIC-D100 ION, CHROMATOGRAPH) were used to quantitatively analyze the contents of bromine and chlorine. The injection time was set at 45 min. The formula for calculating the halogen content in the raw materials is presented as eqn (1).

The contents of chlorine and bromine in the raw materials are calculated using eqn (1):

$$X_0 = \frac{K_0 \times C_0 \times V_0}{M_0} \quad (1)$$

Herein, the dilution factor $K_0 = 10$, V_0 represents the constant-volume value (0.25 L), C_0 denotes the content of chloride and bromide ions in the absorption solution (mg L^{-1}), and M_0 is the mass of the raw material (g).

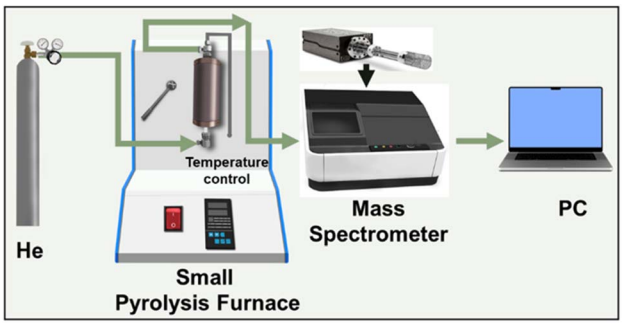

Fig. 1 Online pyrolysis-mass spectrometry apparatus.

The functional group distribution of the raw materials was analyzed using a Fourier-transform infrared spectrometer (Nicolet iS50, Thermo Fisher Scientific, America).

2.3 Thermogravimetry analysis (TG) of PL-NWCCL and FR4-NWPCB

The variation of the raw material mass with temperature was analyzed by a thermogravimetric analyzer (5 Jupiter, NETZSCH, Germany).

2.4 Online pyrolysis-mass spectrometry apparatus and analysis method

The schematic diagram of the online pyrolysis-mass spectrometry apparatus is presented in Fig. 1. The apparatus is composed of a helium (He) gas cylinder, a small – scale pyrolysis furnace, a Sciprecis D-200 model mass spectrometry (MS) instrument, and a computer, and is employed to conduct online monitoring of the volatile organic compounds (VOCs) released during the pyrolysis process. Based on the different thermogravimetric outcomes of the two raw materials, separate testing protocols were formulated, as elaborated in Section 3.2.1. To mitigate the impact of the heat – transfer medium, three isothermal stages were respectively established in the regions where significant weight changes occurred during the pyrolysis of the two materials. For the analysis of PL-NWCCL: a 100 mg sample was used. The heating rate was set at 5 °C min^{-1}, and the final pyrolysis temperature was 600 °C. Isothermal holding periods were respectively arranged at 250 °C, 300 °C, and 350 °C for staged pyrolysis. The full – scan mode was selected, with an m/z range of 1–180 and a scanning rate of 2.5. Regarding the analysis of FR4-NWPCB: a 100 mg sample was taken. The heating rate was 10 °C min^{-1}, and the final pyrolysis temperature was 600 °C. Isothermal holding periods were respectively set at 300 °C, 350 °C, and 400 °C for staged pyrolysis. The full – scan mode was selected, with an m/z range of 1–180 and a scanning rate of 2.5. The release amount of volatile pyrolysis products is denoted by partial pressure (P), with the unit of Torr.

3 Results and discussion

3.1 Raw material analysis

For the PL-NWCCL sample, the material was first cut into pieces of size 4 × 1 cm^2 and then crushed, as depicted in Fig. 2a, and

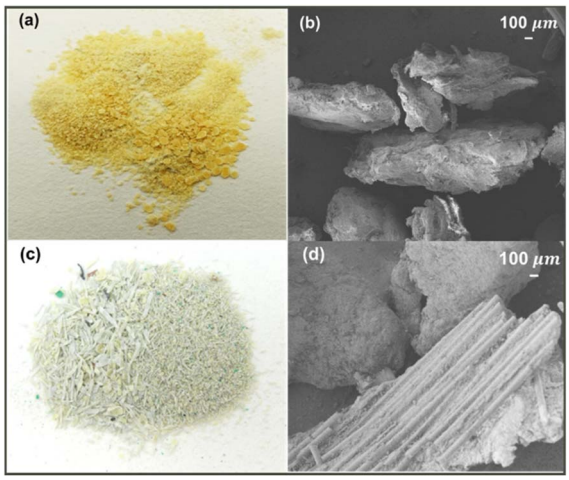

Fig. 2 Material sample; (a) PL-NWCCL. (b) SEM of PL-NWCCL. (c) FR4-NWPCB. (d) SEM of FR4-WPCB.

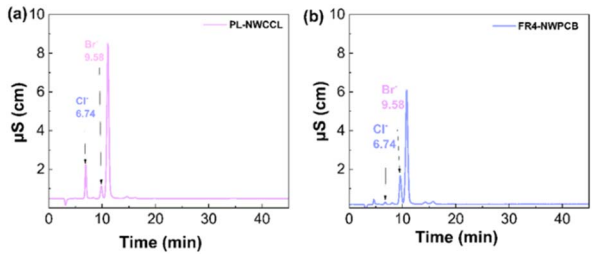

Fig. 3 Ion chromatography analysis. (a) PL-NWCCL. (b) FR4-NWPCB.

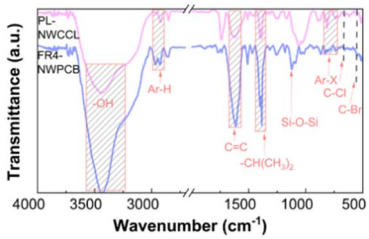

Fig. 4 FTIR of PL-NWCCL and FR4-NWPCB.

the SEM image is presented in Fig. 2b. The FR4-NWPCB is shown in Fig. 2c, and its SEM image is shown in Fig. 2d. Evidently, from Fig. 2b and d, the distinction between glass fiber and resin can be clearly discerned.

3.2 Raw material characterization analysis

3.2.1 Industrial analysis and elemental analysis. The proximate and elemental analyses of PL-NWCCL and FR4-NWPCB are presented in Table 1. As can be seen from the results, the air – dried ash content (Aad) of PL-NWCCL is merely 0.88%, while the air – dried volatile matter content (Vad) is the highest, accounting for 71.83%. In contrast, for FR4-NWPCB, the air – dried ash content (Aad) is the most significant, reaching 64.76%, and the air – dried volatile matter content (Vad) is 30.83%. This indicates that the glass fiber substrate constitutes at least 60% of the non-metallic fraction. Based on the elemental analysis results, the carbon content in PL-NWCCL is 46.22% and the nitrogen content is 4.95%. In FR4-NWPCB, the carbon content is 37.7% and the nitrogen content is 1.61%. These findings suggest that a nitrogen – containing curing agent was incorporated into the resin. Further analysis is required to identify the specific substance.

3.2.2 Ion chromatography analysis of PL-NWCCL and FR4-NWPCB. Ion chromatography analysis was performed on PL-NWCCL and FR4-NWPCB[40] and the resulting ion chromatograms are presented in Fig. 3, which indicates that these two raw materials contain both brominated and chlorinated flame retardants. By applying eqn (1), the bromine content in PL-NWCCL was 21.962 mg g^{-1}, and the chlorine content was 21.154 mg g^{-1}. For FR4-NWPCB, the bromine content was 43.743 mg g^{-1}, and the chlorine content was 8.477 mg g^{-1}. These results confirm that both PL-NWCCL and FR4-NWPCB contain brominated and chlorinated flame retardants.

3.2.3 FTIR analysis of PL-NWCCL and FR4-NWPCB. The Fourier-transform infrared (FTIR) spectra of PL-NWCCL and FR4-NWPCB are depicted in Fig. 4. As is evident from Fig. 4, the primary functional groups of the two materials are presented in Table 2. The peaks at 1399 cm^{-1} and 1384 cm^{-1} are characteristic of the $-CH(CH_3)_2$ group within the isopropyl moiety. Consequently, within the major functional groups, there exists a branched alkyl chain that is linked to the main chain *via* a central carbon atom and bears two methyl substitutions. The peak at 472 cm^{-1} is indicative of the stretching vibration of the C–Br bond.[37] Owing to the existence of the C–Br bond, some benzene ring skeletons associated with this carbon atom, along with the out-of-plane bending vibration of C–H, shift in the direction of lower wave numbers. So, the peak at 1510 cm^{-1} corresponds to the vibrational characteristic of the C=C bond in the benzene ring. The peaks at 813 cm^{-1} and 739 cm^{-1} can be ascribed to the out-of-plane deformation vibration (γ = C–H) and in-plane deformation vibration (δ)[41] of substituted benzene, respectively. Meanwhile, Consequently, based on the above-mentioned peaks of functional groups, it can be firmly established that the brominated flame retardant incorporated established that the brominated flame retardant incorporated

Table 1 Elemental and proximate analysis of PL-NWCCL and FR4-NWPCB

	Proximate analysis (wt%)				Elemental analysis (wt%)			
	M_{ad}	A_{ad}	V_{ad}	FC_{ad}	C/wt%	H/wt%	N/wt%	S/wt%
PL-NWCCL	3.41	0.88	71.83	23.88	46.22	4.02	4.95	0.13
FR4-NWPCB	1.67	64.76	30.83	2.74	37.70	4.34	1.61	0.11

Table 2 Primary functional groups of PL-NWCCL and FR4-NWPCB

The types of bonds	PL-NWCCL/cm^{-1}	FR4-NWPCB/cm^{-1}
–OH	3427	3427
C_{sp^3}–H	2923	2970/2927
Ester C=O	1739	1765/1746
C=C	1626	1613
Benzene ring	1510	1503
$CH(CH_3)_2$	1399/1384	1399/1384
C–O bonds	1245	1245
Si–O–Si	—	1115
Aliphatic amines	1044/1016	1044/1016
SO_2	1256	1256
S=O	1038	1038
Para-substitution	813	867
Ortho substitution on the benzene ring	739	739
C–Cl	659	659
C–Br	472	472

in both PL-NWCCL and FR4-NWPCB is tetrabromobisphenol A (TBBPA).[28] The peak at 2923 cm^{-1} is associated with the stretching vibration of Csp^3–H,[26] and the peak at 659 cm^{-1} represents the stretching vibration of the C–Cl bond.Thus, it can be deduced that both PL-NWCCL and FR4-NWPCB contain chlorinated flame retardants. However, the exact type thereof remains to be further determined in subsequent investigations. The peak at 1739 cm^{-1} is attributed to the stretching vibration of the carboxyl group (ν(C=O)) in the curing agent. The peaks at 1044 cm^{-1} and 1016 cm^{-1} correspond to the stretching vibrations of the C–N bond in aliphatic amines.[42] Additionally, considering the stretching vibration of SO_2 represented by the peak at 1256 cm^{-1} and the stretching vibration of S=O denoted by the peak at 1038 cm^{-1},[43] it can be comprehensively confirmed that the added chlorinated flame retardant is 4,4′-diaminodiphenyl sulfone (abbreviated as DDS).The peak at 3427 cm^{-1} can be assigned to the stretching vibration of the free hydroxyl group (ν(O–H)) in alcohols or phenols.[26] The peak at 1233 cm^{-1} corresponds to the stretching vibration of the C–O bond in aliphatic ethers. These functional groups are situated in the end chains or cross-linking groups of the resin. Notably, the peak at 1115 cm^{-1} in FR4-NWPCB corresponds to the antisymmetric stretching vibration of Si–O–Si.[1,7,43] In contrast, PL-NWCCL does not exhibit a prominent peak at this location. The presence of the Si–O–Si bond represents the most substantial distinction between these two materials.

3.3 TG analysis of PL-NWCCL and FR4-NWPCB

An analysis was conducted on the pyrolysis characteristics of PL-NWCCL and FR4-NWPCB under different heating rates. The thermogravimetric (TG) curve of PL-NWCCL is presented in Fig. 5a, and the derivative thermogravimetric (DTG) curve is shown in Fig. 5c. The TG curve of FR4-NWPCB is depicted in Fig. 5b, and the DTG curve is illustrated in Fig. 5d.

As can be seen from Fig. 5a and b, the thermogravimetric (TG) curves of PL-NWCCL and FR4-NWPCB both exhibit a rightward shift with the increase in the heating rate.[44] This phenomenon can be attributed to the delay in heat conduction at a higher heating rate, which results in the pyrolysis process taking a longer time to be completed.[45] For PL-NWCCL, when the heating rates are set at 10 °C min^{-1} and 15 °C min^{-1}, the TG curves of their pyrolysis show an overall upward deviation compared to the curve at 5 °C min^{-1}. This indicates that the final weight loss rate reaches its maximum value under the condition of a heating rate of 5 °C min^{-1}. For FR4-NWPCB, in comparison with heating rates of 5 °C min^{-1} and 15 °C min^{-1}, the pyrolysis interval at 10 °C min^{-1} is the broadest. The pyrolysis is also the most thorough and requires a relatively shorter time.[46] In summary, a heating rate of 5 °C min^{-1} is selected for the pyrolysis of PL-NWCCL, while a heating rate of 10 °C min^{-1} chosen for the pyrolysis of FR4-NWPCB.

The pyrolysis characteristic parameters of PL-NWCCL and FR4-NWPCB are presented in Table 3. As indicated by Table 2, the primary weight-loss temperature range of PL-NWCCL is 233–550 °C, whereas that of FR4-NWPCB is 300–400 °C. Evident from Fig. 5c and d, there are notable discrepancies in the DTG curves of the two materials. Under a heating rate of 5 °C min^{-1}, PL-NWCCL underwent its first stage of weight-loss within the temperature range of 250–350 °C. The pyrolysis reaction reached its maximum intensity at 311 °C. Subsequently, the material entered the second weight-loss stage within the temperature range of 420–530 °C, thereby undergoing further decomposition. This suggests that the poorly volatile components undergo further decomposition. Consequently, the corresponding DTG curve exhibits another relatively minor weight-loss peak at this location. In the case of FR4-NWPCB, complete weight loss is achieved after 420 °C, and its associated DTG curve features only a single weight-loss peak.

3.4 Online pyrolysis-MS analysis of PL-NWCCL and FR4-NWPCB

3.4.1 Mass spectrometry identification. Taking the mass spectrometry of PL-NWCCL and FR4-NWPCB at 300 °C, the

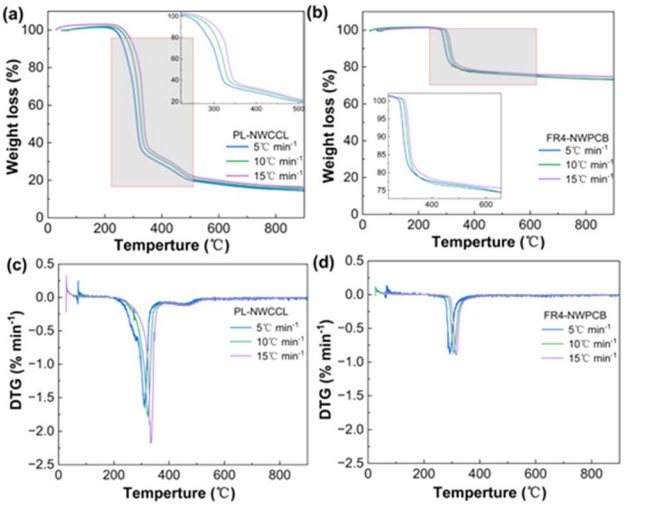

Fig. 5 TG and DTG. (a) TG of PL-NWCCL. (b) TG of FR4-NWPCB. (c) DTG of PL-NWCCL. (d) DTG of FR4-NWPCB.

Table 3 The pyrolysis characteristic parameters of PL-NWCCL and FR4-NWPCB under different heating rates

Material	Heating rate/°C min^{-1}	Starting temperature/°C	Peak temperature/°C	Final temperature/°C	Weight loss/%
PL-NWCCL	5	233	311	331	85.52
	10	245	323	344	84.44
	15	267	333	355	83.36
FR4-NWPCB	5	280	293	376	26.95
	10	292	306	422	26.83
	15	301	315	398	25.35

temperature at which the pyrolysis reaction is most intense, as an example, these spectra were compared with the standard mass spectrometry data in the NIST database (Table S1). The RGASoft software (version 4.3.0) was employed to identify and characterize the volatile products according to the *m*/*z* values and intensities of the molecular ion peaks. The results show that the pyrolysis volatile products include chlorinated compounds,[35,47] brominated compounds,[48–50] phenolic compounds, hydrocarbon compounds, ether compounds, ketone compounds,[27,38,51,52] as well as the pyrolysis products of cellulose[53–55] and DDS[43] (Fig. S2–S8).

3.4.1.1 Chlorinated compounds. Regarding the types of chlorinated flame retardants,[35,47] the primary approach to differentiating between PVC and chlorinated alkanes in mass spectrometry is by identifying their pyrolysis products. HCl and CH_3Cl are common products of both substances. During the pyrolysis of PVC, potential chlorinated compounds include C_2H_3Cl, C_3H_5Cl, C_4H_7Cl, and C_5H_9Cl.[54,56,57] For chlorinated alkanes, the products may include C_2H_5Cl, C_3H_7Cl, C_4H_9Cl, $C_5H_{11}Cl$, and C_6H_5Cl.[58] Identification was carried out by analyzing the intensity ratios of fragment ions corresponding to the *m*/*z* values of molecular ion peaks and the isotopic distribution of Cl. The chlorinated compounds generated during the pyrolysis of PL-NWCCL and FR4-NWPCB at 300 °C are presented in Fig. 6a and b. As depicted in Fig. 6a and b , the characteristic Cl^- isotopic peaks (*m*/*z* values of 35/37 with an intensity ratio of 3 : 1) and the isotopic peak clusters of chlorinated alkanes[59,60] such as CH_3Cl, C_3H_7Cl, C_4H_9Cl, and $C_5H_{11}Cl$ were detected in the pyrolysis products of both raw materials. During the pyrolysis of FR4-NWPCB, the amount of HCl generated was so minimal that it was nearly undetectable. The pyrolysis products of PL-NWCCL were found to contain HCl, C_2H_5Cl, and C_3H_5Cl, which may be attributed to the presence of cellulose within it. During the pyrolysis process, cellulose and chlorinated substances can yield 4-chloro-2-butanone[35] (with ion fragments having *m*/*z* values of 43, 27, and 71). However, as the intensity of the 71-ion fragment in the obtained mass spectrum did not align with the peak intensity in the standard mass spectrum data (see Table S1), it indicates that 4-chloro-2-butanone was not detected in the pyrolysis products at 300 °C. This could potentially be due to the fact that 4-chloro-2-butanone is prone to decomposition after its formation.

Chlorinated alkanes do not possess a fixed structural formula, and chlorine (Cl) is not uniformly substituted during the synthesis process.[61] Therefore, for the purpose of further analysis, based on the content and average chlorination degree of short-chain chlorinated paraffins in industrial and environmental samples, their chemical formula is denoted as $C_{12}H_{19}Cl_7$.[62,63]

3.4.1.2 Brominated compounds. The identification results of the bromine-containing compounds produced during the pyrolysis of PL-NWCCL and FR4-NWPCB at 300 °C are presented in Fig. 6c and d. As is evident from Fig. 6c and d, both mass spectra exhibit isotope peak patterns at *m*/*z* 79/81 (the Br-isotope doublet with an intensity ratio of 1 : 1) and *m*/*z* 94/96 (the $[M]^+$ and $[M + 2]^+$ molecular ion peaks of CH_3Br). When combined with the ion fragment at *m*/*z* 15 (CH_3^+), it can be deduced that both PL-NWCCL and FR4-NWPCB generate HBr and CH_3Br during the pyrolysis process. Furthermore, in the mass spectrum of FR4-NWPCB, a series of additional fragments were detected, including *m*/*z* 108/110 (the $[M]^+/[M + 2]^+$ peaks of C_2H_5Br), 27 ($C_2H_3^+$), 29 ($C_2H_5^+$), and 57.0 ($C_3H_5O^+$). Consequently, the bromine-containing compounds in the pyrolysis products of FR4-NWPCB also include C_2H_5Br and C_3H_5BrO.

3.4.1.3 Phenolic compounds. The release characteristics of phenolic compounds are closely associated with the type of resin matrix. The distinction between epoxy resin and phenolic resin lies in their distinct characteristic phenolic products. During pyrolysis, phenolic resin yields o/m-cresol (C_7H_8O),[3] whereas epoxy resin predominantly generates p-cresol (designated as C_7H_8O-1) and p-isopropylphenol ($C_9H_{12}O$).[4] The identification results of the phenolic compounds produced during

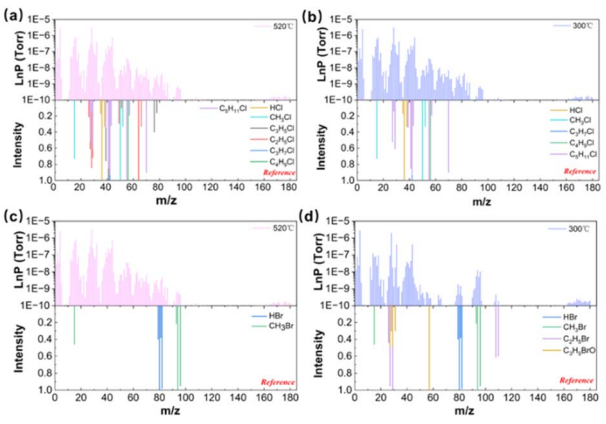

Fig. 6 Mass spectrometry identification of halogen compounds. (a) Chlorinated compounds of PL-NWCCL. (b) Chlorinated compounds of FR4-NWPCB; (c) brominated compounds of PL-NWCCL. (d) Brominated compounds of FR4-NWPCB.

the pyrolysis of PL-NWCCL and FR4-NWPCB at 300 °C are presented in Fig. 7a and b. As is apparent from Fig. 7a and b, the peaks at *m*/*z* 94 ($[M]^+$, $C_6H_6O^+$) and 65 ($C_5H_5O^+$) are the characteristic peaks of phenol (C_6H_6O). The peaks at *m*/*z* 108 ($[M]^+$, $C_7H_8O^+$), 107 ($[M–H]^+$), and 77 ($C_6H_5^+$) are the characteristic peaks of p-cresol (C_7H_8O-1). Thus, the resins contained in both PL-NWCCL and FR4-NWPCB are epoxy resins. Simultaneously, the peaks at *m*/*z* 91 ($C_7H_7^+$) and 77 ($C_6H_5^+$) are the characteristic peaks of $C_9H_{12}O$. This indicates that $C_9H_{12}O$ is also present in the pyrolysis phenolic products of these two raw materials.

3.4.1.4 Hydrocarbon compounds. Since hydrocarbon compounds[27,38,51,52] are the products of the further pyrolysis of TBBPA and TBBA, the identification results of the hydrocarbon compounds produced during the pyrolysis of PL-NWCCL and FR4-NWPCB at 300 °C are presented in Fig. 7c and d. As depicted in Fig. 7c and d, characteristic peaks at *m*/*z* 78 (the molecular ion peak $[M]^+$ of C_6H_6) and *m*/*z* 91/92 (the molecular ion peaks $[M–H]^+$/$[M]^+$ of C_7H_8) are present in both mass spectra. Consequently, the hydrocarbon compounds released during the pyrolysis process of PL-NWCCL and FR4-NWPCB are C_6H_6 and C_7H_8.

3.4.1.5 Ethers and ketones compounds. The identification results of the ether compounds produced during the pyrolysis of PL-NWCCL and FR4-NWPCB at 300 °C are presented in Fig. 8a and b. As can be observed, in both mass spectra, molecular ion peaks at *m*/*z* 45 ($[M–CH_3]^+$, $C_2H_5O^+$), 60 ($[M]^+$), and 59 ($[M–H]^+$, $C_3H_7O^+$) are present. These are the characteristic peaks of C_3H_8O. Additionally, molecular ion peaks at *m*/*z* 89 ($[M–CHO]^+$, $C_7H_5^+$) and *m*/*z* 90 ($[M–CO]^+$, $C_7H_6^+$) are evident, which are characteristic of C_8H_6O. Consequently, the ether compounds released during the pyrolysis processes of both PL-NWCCL and FR4-NWPCB are C_3H_8O and C_8H_6O. In the mass spectrum of FR4-NWPCB, molecular ion peaks at *m*/*z* 45 ($[M]^+$) and 74 ($C_2H_5O^+$) were also detected. This indicates that $C_4H_{10}O$ is also among the pyrolysis ether products of FR4-NWPCB.

The identification results of the ketone compounds produced during the pyrolysis of PL-NWCCL and FR4-NWPCB at 300 °C are presented in Fig. 8c and d. Upon examination, the peaks at *m*/*z* 29 ($[M–CH_3]^+$, CHO^+), 43 ($[M^+ H–H_2O]^+$, $C_2H_3^+$), and 44 ($[M^+ H]^+$) are characteristic of C_2H_4O. Meanwhile, the peaks at *m*/*z* 58 ($[M]^+$), 43 ($[M–CH_3]^+$, $C_2H_3O^+$), and 15 (CH_3^+) are characteristic of C_3H_6O. Consequently, the ketone compounds generated during the pyrolysis of PL-NWCCL and FR4-NWPCB are C_2H_4O and C_3H_6O.

3.4.1.6 Pyrolysis products of DDS and cellulose. The identification results of the substances potentially generated from the pyrolysis of DDS[43] added to PL-NWCCL and FR4-NWPCB at 300 °C are presented in Fig. 8e and f. As can be discerned, the peaks at *m*/*z* 39 ($C_3H_3^+$), 65 ($[M–C_2H_2]^+$, $C_4H_3N^+$), and 93 ($[M]^+$) are characteristic of C_6H_7N. The peaks at *m*/*z* 41 ($C_3H_5^+$), 47 ($[M–C_2H_5]^+$, HS^+), and 76 ($[M]^+$) are characteristic of C_3H_8S. Consequently, the pyrolysis products of DDS in PL-NWCCL and FR4-NWPCB are C_6H_7N and C_3H_8S.

Particularly, the main substance of the substrate wood pulp paper in PL-NWCCL is cellulose.[50,56,57] During the pyrolysis process, cellulose can also undergo decomposition. The identification results of its pyrolysis products at 300 °C are presented in Fig. 8e. The molecular ion peaks at *m*/*z* 60.0 ($[M]^+$), 43 ($[M–OH]^+$, $C_2H_3O^+$), and 45 ($[M–CH_3]^+$) are characteristic of acetic acid (designated as $C_2H_4O_2$-1). Meanwhile, the peaks at *m*/*z* 31 ($[M + H–2H_2O]^+$, CH_3O^+), 29 ($[M–CH_2O]^+$, CHO^+), and 32 ($[M + H–H_2O]^+$) are characteristic of hydroxy-acetaldehyde (designated as $C_2H_4O_2$-2). Consequently, the pyrolysis products of cellulose in PL-NWCCL are $C_2H_4O_2$-1 and $C_2H_4O_2$-2.

3.4.2 Release patterns of halogens during the pyrolysis. The release patterns of halogens during the pyrolysis of PL Consequently, the pyrolysis products of cellulose inNWCCL are presented in Fig. 9a and b. Fig. 9a relates to chlorinated

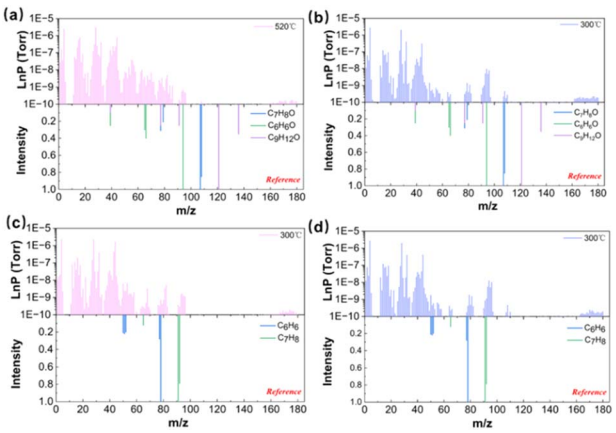

Fig. 7 Identification of phenolic compounds and hydrocarbon compounds. (a) Phenolic compounds of PL-NWCCL. (b) Phenolic compounds of FR4-NWPCB. (c) Hydrocarbon compounds of NWCCL. (d) Hydrocarbon compounds of FR4-NWPCB.

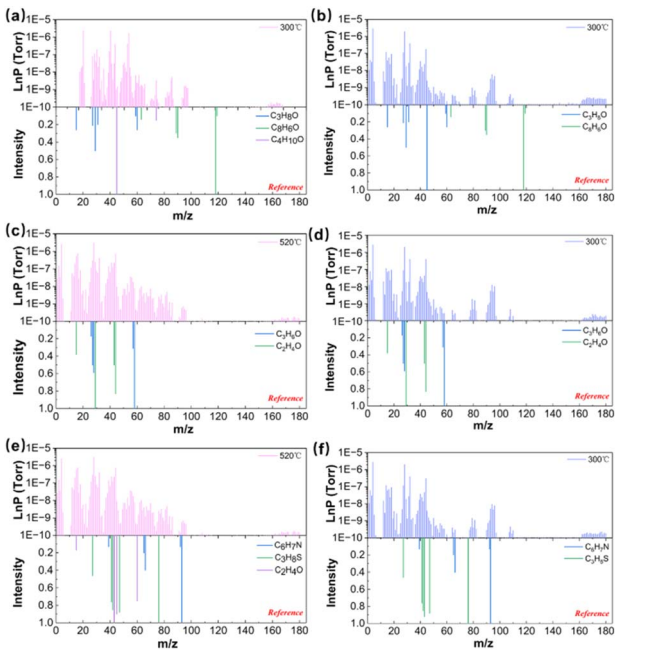

Fig. 8 Ethers compounds, ketones compounds and pyrolysis products of DDS and cellulose, PL-NWCCL: (a), (c), (e). FR4-NWPCB: (b), (d), (f).

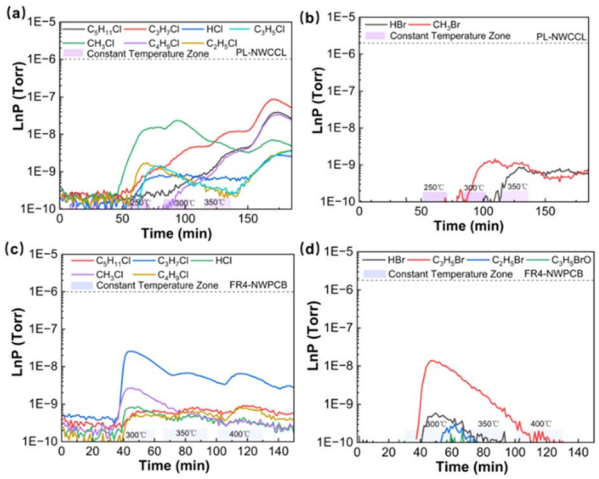

Fig. 9 Pyrolysis products of halogenated flame retardants of PL-NWCCL and FR4-NWPCB; PL-NWCCL: (a) chlorinated compounds, (b) brominated compounds; FR4-NWPCB: (c) chlorinated compounds, (d) brominated compounds.

compounds, and Fig. 9b relates to brominated compounds. As shown in Fig. 9a, the release of CH_3Cl commences at 240 °C. Its release quantity reaches a maximum of 2.39×10^{-8} Torr at 300 °C and then gradually declines. Even at 520 °C, CH_3Cl continues to be released, although the release quantity has dropped to 0.39×10^{-8} Torr. C_3H_7Cl begins to be emitted when the pyrolysis temperature reaches 250 °C. C_2H_5Cl and HCl start to be generated successively after the 10th minute of the holding stage. C_3H_5Cl starts to be generated after the 12th minute, with a relatively small production amount. C_4H_9Cl and $C_5H_{11}Cl$ start to be released at 300 °C. Subsequently, the release amounts of HCl, C_2H_5Cl, C_3H_5Cl, C_3H_7Cl, C_4H_9Cl, and $C_5H_{11}Cl$ gradually increase as the temperature rises. And these compounds reach their maximum release amounts at 520 °C and then gradually decrease.

During the holding stage at 250 °C, the chlorinated flame retardants incorporated in PL-NWCCL started to decompose. Among these, CH_3Cl was the first to be released. By the end of the holding stage, its emission amount reached 1.47×10^{-8} Torr. Subsequently, C_2H_5Cl, HCl, and C_3H_7Cl were successively emitted, with emission amounts of 1.5×10^{-9} Torr, 0.7×10^{-9} Torr, and 0.9×10^{-9} Torr, respectively, at the end of the holding stage. Finally, C_3H_5Cl began to be emitted in small quantities, and its emission amount was 0.10×10^{-8} Torr by the end of the holding stage.

During the holding stage at 300 °C, the emission amount of CH_3Cl increased to a maximum value of 2.39×10^{-8} Torr and then gradually declined. By the end of the holding stage, it dropped to 1.68×10^{-8} Torr. The emission amount of C_3H_7Cl continuously increased from 0.14×10^{-8} Torr to 0.42×10^{-8} Torr. C_2H_5Cl and C_3H_5Cl exhibited consistent emission trends but with different amount numbers. The emission amount of C_2H_5Cl decreased from 0.11×10^{-8} Torr to 0.6×10^{-8} Torr, while that of C_3H_5Cl decreased from 0.13×10^{-8} Torr to 0.4×10^{-9} Torr. In addition, C_4H_9Cl and $C_5H_{11}Cl$ started to be emitted. By the end of the holding stage, their emission amounts reached 0.4×10^{-9} Torr and 0.6×10^{-9} Torr, respectively. Throughout this stage, the emission amount of HCl remained constant at 0.6×10^{-9} Torr.

During the holding stage at 350 °C, the emission amount of CH_3Cl decreased continuously from 0.84×10^{-8} Torr to 0.43×10^{-8} Torr. In contrast, the emission amount of C_3H_7Cl increased from 0.47×10^{-8} Torr to 1.17×10^{-8} Torr. The emission amounts of C_4H_9Cl and $C_5H_{11}Cl$ increased from 0.06×10^{-8} Torr and 0.8×10^{-9} Torr to 0.30×10^{-8} Torr and 0.34×10^{-8} Torr, respectively. During this period, the emission amounts of HCl, C_2H_5Cl, and C_3H_5Cl all decreased slightly.

As the pyrolysis temperature increased, at 423 °C, the emission amounts of CH_3Cl, C_2H_5Cl, C_3H_5Cl, C_3H_7Cl, C_4H_9Cl, and $C_5H_{11}Cl$ all started to rise. The emission amount of CH_3Cl increased slightly by 0.39×10^{-8} Torr at 514 °C and then began to decline. The emission amounts of HCl, C_3H_7Cl, C_4H_9Cl, and $C_5H_{11}Cl$ reached their maximum values (0.27×10^{-8} Torr, 8.65×10^{-8} Torr, 3.37×10^{-8} Torr, and 3.95×10^{-8} Torr, respectively) at 530 °C and then decreased as the temperature further increased. The emission amounts of C_2H_5Cl and C_3H_5Cl continued to increase slightly with the increasing temperature. At 600 °C, their emission amounts were 0.35×10^{-8} Torr and 0.37×10^{-8} Torr, respectively. In contrast, the emission amount of C_6H_5Cl was extremely low and was scarcely detectable within the temperature range up to 600 °C.

Therefore, it can be deduced that during the pyrolysis process of PL-NWCCL, after the carbon–carbon bonds of chlorinated alkanes are broken, Cl· radicals tend to combine with CH_3· to form CH_3Cl. Subsequently, they react with C_2H_5·, C_3H_7·, and H· to yield C_2H_5Cl, C_3H_7Cl, and HCl, respectively. Thereafter, Cl· radicals combine with C_3H_5· to form C_3H_5Cl. As the temperature increases, Cl· radicals are also capable of reacting with C_4H_9· and C_5H_{11}· to generate C_4H_9Cl and $C_5H_{11}Cl$. Additionally, the cellulose in the wood pulp paper participates in reactions, which significantly reduces the emission of HCl and decreases the dechlorination efficiency.[35,54] When the pyrolysis temperature is further elevated to 470–530 °C, PL-NWCCL undergoes a secondary mass loss process. Simultaneously, Cl· groups begin to be generated again and combine with hydrocarbon groups to form chlorinated hydrocarbons.

The release profiles of brominated compounds in PL-NWCCL are presented in Fig. 9b. As depicted in the figure, no emission of brominated compounds was observed during the holding stage at 250 °C. CH_3Br started to be emitted at 285 °C, and HBr began to be released at the 19th minute of the 300 °C holding stage. The maximum partial pressure of the release amount of HBr during the 300 °C holding stage was 0.9×10^{-9} Torr. For CH_3Br, its release amount reached a maximum of 0.15×10^{-8} Torr at 320 °C. Subsequently, the release amounts of both continued to be emitted in relatively small quantities as the temperature increased.

During the pyrolysis of PL-NWCCL, the release pattern of bromine differs from that of chlorine. The amount of bromine released during the second weight-loss interval remains relatively constant. In brominated epoxy resins, the brominated

part exhibit lower thermal stability compared to the non-brominated part. Consequently, the debromination process and the cleavage of brominated structures occur prior to the breakdown of non-brominated structures.[26] Thus, when the pyrolysis temperature reaches 300 °C, the C–Br bond preferentially breaks. The resulting Br· radicals preferentially combine with CH_3· radicals to form CH_3Br, which is then released. Subsequently, Br· radicals also react with H· radicals to form HBr molecules, which are likewise released.[48,64] In the context of radical-based pyrolysis reactions, Br· radicals dissociated from tetrabromobisphenol A tend to associate with short-chain alkyl radicals generated during the pyrolysis process.[16] After 350 °C, as the temperature rises, a small quantity of brominated compounds continues to be released. The release amount remains relatively stable within the temperature range of 470–530 °C.

Fig. 9c and d depict the release patterns of halogenated flame retardants in FR4-NWPCB. Specifically, Fig. 9c focuses on chlorinated compounds, and Fig. 9d on brominated compounds. As can be observed from Fig. 9c, the release of CH_3Cl commences when the temperature reaches 300 °C. 4 minutes later, C_3H_7Cl begins to be emitted. After an additional 8 minutes, HCl, C_4H_9Cl, and $C_5H_{11}Cl$ are successively released. All these compounds reach their maximum release amounts during the holding stage at 300 °C. After reaching 400 °C, small amounts of C_3H_7Cl, C_4H_9Cl and $C_5H_{11}Cl$ are still released.

During the holding stage at 300 °C, the release patterns of CH_3Cl and C_3H_7Cl were consistent. Their release rates increased sharply at the 6th minute. At the 15th minute, they reached maximum amounts of 0.25×10^{-8} Torr and 2.57×10^{-8} Torr, respectively, after which the release amounts decreased rapidly. HCl, C_4H_9Cl, and $C_5H_{11}Cl$ reached their maximum release levels at the 19th minute of the holding stage, with values of 0.7×10^{-9} Torr, 0.5×10^{-9} Torr, and 0.9×10^{-9} Torr, respectively. As the pyrolysis temperature increased, the release amounts of C_3H_7Cl, HCl, and C_4H_9Cl increased slightly during the holding stages at 350 °C and 400 °C. The release amounts of CH_3Cl and $C_5H_{11}Cl$ decreased with rising temperature, and C_6H_5Cl was scarcely detectable. In conclusion, during the pyrolysis process, Cl· radicals tend to combine with CH_3· and C_3H_7· groups. Moreover, most of the Cl-containing substances were removed at 400 °C.[48]

As depicted in Fig. 9d, the release of CH_3Br commenced at the 5th minute of the 300 °C holding stage, while that of HBr started at the 10th minute. Once the pyrolysis temperature reached 400 °C, both substances were essentially released completely. During the 300 °C holding stage, the release rate of CH_3Br increased rapidly to 1.39×10^{-8} Torr at the 8th minute. Subsequently, as the pyrolysis temperature continued to increase, its release amount gradually decreased. The release amount of HBr increased to a maximum of 0.3×10^{-9} Torr at 300 °C and then decreased gradually. The release amount of C_3H_5BrO during the 300 °C holding stage was relatively low, measuring 0.1×10^{-9} Torr, and no release was detected after 400 °C. During the pyrolysis process, the release patterns of chlorinated compounds in FR4-NWPCB deviated significantly from those in PL-NWCCL. This discrepancy can be attributed to

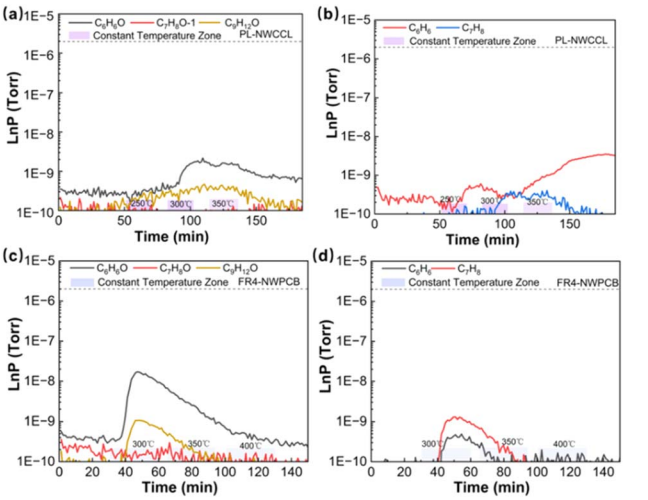

Fig. 10 Phenolic compounds and hydrocarbon compounds of PL-NWCCL and FR4-NWPCB; PL-NWCCL: (a) phenolic compounds, (b) hydrocarbon compounds; FR4-NWPCB: (c) phenolic compounds, (d) hydrocarbon compounds.

the differences in their substrates.[65] After 400 °C, the halogen flame retardants in FR4-WPCB were scarcely released. In contrast, the release patterns of bromine-containing compounds during the pyrolysis of the two materials were consistent. The majority of these compounds were completely released within the temperature range of 300–350 °C.

3.4.3 Release pattern of other products. Fig. 10a and b present the release patterns of phenolic compounds and hydrocarbon compounds, respectively, among the pyrolysis products of PL-NWCCL. As is evident from Fig. 10a, both C_6H_6O and $C_9H_{12}O$ started to be released simultaneously at the 9th minute of the 250 °C holding stage, albeit in minimal quantities. As the temperature increased, the release amounts of C_6H_6O and $C_9H_{12}O$ peaked at 322 °C, reaching 0.22×10^{-8} Torr and 0.5×10^{-9} Torr, respectively. After the conclusion of the 350 °C holding stage, their release amounts gradually declined. The remaining phenolic pyrolysis products were only sparingly released at 350 °C and 423 °C.

As depicted in Fig. 10b, the principal hydrocarbon products in the pyrolysis products of PL-NWCCL are C_6H_6 and C_7H_8, and both are released in minute quantities. C_6H_6 and C_7H_8 commence their release at the 9th minute of the 250 °C holding stage. By the conclusion of this holding stage, their release amounts are 0.4×10^{-9} Torr and 0.1×10^{-9} Torr, respectively. As the temperature rises, C_7H_8 attains its maximum release amount of 0.4×10^{-9} Torr at 300 °C and then starts to decline. C_6H_6 reaches its peak release amount of 0.35×10^{-8} Torr at 530 °C and subsequently decreases as the temperature continues to increase. Consequently, the release patterns of phenolic products and the pyrolysis products of bromine-containing flame retardants generated during the pyrolysis of PL-NWCCL are largely consistent. Moreover, aromatic hydrocarbons will undergo further decomposition and release during the second weight-loss stage of the pyrolysis process.[66]

Fig. 10c and d illustrate the release patterns of phenolic compounds and hydrocarbon compounds, respectively, in the pyrolysis products of FR4-NWPCB. As is evident from Fig. 10c, both C_6H_6O and $C_9H_{12}O$ initiate their release at the 7th minute of the 300 °C holding stage. The release amount of C_6H_6O peaks at 1.71×10^{-8} Torr at the 17th minute and subsequently decreases as the pyrolysis temperature rises. For $C_9H_{12}O$, its release amount reaches a maximum of 0.11×10^{-8} Torr at the 17th minute and then gradually declines. C_7H_8O starts to be released at the 20th minute of the 300 °C holding stage. By the end of this holding stage, its release amount reaches a maximum of 0.5×10^{-9} Torr, after which it gradually decreases. From Fig. 10d, it can be seen that C_6H_6 and C_7H_8 begin to be released at the 10th minute of the 300 °C holding stage. Their release amounts reach maximum values at the 20th minute, specifically 0.4×10^{-9} Torr for C_6H_6 and 0.13×10^{-8} Torr for C_7H_8. Subsequently, their release amounts decrease with increasing temperature, and they are completely released at 350 °C.

There are also distinctions in the release patterns of phenolic compounds and hydrocarbon compounds generated during the pyrolysis of PL-NWCCL and FR4-NWPCB. For PL-NWCCL, the majority of the phenolic compounds are fully released at 350 °C. Only C_6H_6O continues to be released in minor quantities. Around 500 °C, the poorly-volatile components in PL-NWCCL undergo further decomposition, which leads to the further release of hydrocarbon products. In contrast, for FR4-NWPCB, both the phenolic compounds and hydrocarbon compounds are predominantly released completely within the temperature range of 300–400 °C.

Fig. 11a–c depict the release patterns of ether compounds, ketone compounds, nitrogen-containing compounds, and pyrolysis products of cellulose during the pyrolysis of PL-NWCCL. As is evident from Fig. 11a, C_8H_6O initiated its release at the 10th minute of the 300 °C holding stage, whereas C_3H_8O started to be released at the conclusion of the 300 °C holding stage. The lease amount of C_8H_6O peaked at 0.2×10^{-9} Torr at 350 °C and subsequently declined gradually. For C_3H_8O, its release amount reached a maximum of 0.5×10^{-9} Torr at 510 °C and then gradually decreased. $C_4H_{10}O$ commenced its release after the end of the 350 °C holding stage and continued to be released during the process of heating up to 600 °C.

As can be seen from Fig. 11b, the primary ketone products released from PL-NWCCL are C_2H_4O and C_3H_6O. C_2H_4O commences its release at the onset of the 250 °C holding stage. Five minutes later, C_3H_6O also begins to be released. The release trends of both substances remain congruent prior to 300 °C. The release amount of C_3H_6O attains its maximum value of 0.75×10^{-8} Torr at 508 °C and subsequently starts to decline. For C_2H_4O, its release amount reaches a peak of 12.86×10^{-8} Torr at 533 °C and then begins to decrease. Fig. 11c reveals that $C_2H_4O_2$, the main pyrolysis product of cellulose, starts to be released at 250 °C. Its release amount increases until it reaches a maximum of 2.53×10^{-8} Torr at 300 °C and then gradually diminishes. The pyrolysis product of DDS, C_3H_8S, begins to be released in trace amounts at 250 °C. During the 300 °C holding stage, it continues to be released and reaches a maximum of 0.2×10^{-8} Torr. Another pyrolysis product of DDS, C_6H_7N, starts to be released during the 300 °C holding stage, with the release amount remaining at 0.15×10^{-8} Torr. Subsequently, the release amounts of both substances gradually decrease as the temperature increases.

Fig. 11d–f depict the release patterns of ether compounds, ketone compounds, and nitrogen-containing compounds generated during the pyrolysis of FR4-WPCB. As is evident from Fig. 11d, C_8H_6O started to be released rapidly at the 9th minute of the 300 °C holding stage. It reached a maximum release amount of 0.04×10^{-8} Torr at the 23rd minute and subsequently decreased gradually. The release amount of C_3H_8O at 350 °C was extremely low, merely 0.5×10^{-10} Torr. From Fig. 11e, it can be seen that although the release amount of C_2H_4O during the pyrolysis process generally remained in the

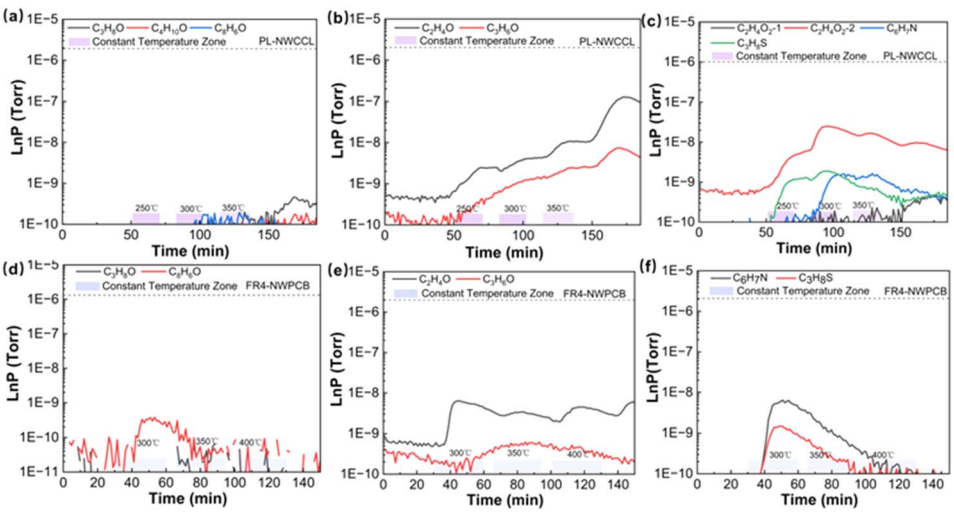

Fig. 11 Ether compounds, ketone compounds, nitrogen-containing compounds, and pyrolysis products of cellulose of PL-NWCCL and FR4-NWPCB; PL-NWCCL: (a) ether compounds, (b) ketone compounds, (c) nitrogen-containing compounds, and pyrolysis products of cellulose; FR4-NWPCB: (d) ether compounds, (e) ketone compounds, (f) nitrogen-containing compounds.

range of 0.2–0.6 × 10^{-8} Torr as the temperature rose, within each of the three holding stages, its release amount exhibited a pattern of a slight increase followed by a decrease. C_3H_6O began to be released in small quantities starting from 300 °C, and its release amount remained at 0.6 × 10^{-9} Torr until the conclusion of the pyrolysis. As presented in Fig. 11f, C_3H_8S and C_6H_7N initiated rapid release simultaneously during the 300 °C holding stage. Within 10 minutes, they reached maximum release amounts of 0.14 × 10^{-8} Torr and 0.64 × 10^{-8} Torr, respectively. Thereafter, their release amounts gradually decreased as the pyrolysis temperature increased.

3.5 The formation mechanism of volatile pyrolysis products of PL-NWCCL and FR4-NWPCB

Through the detection and analysis of pyrolysis volatile products, and in conjunction with the bond energies of raw materials as presented in Table S2, it can be observed that the migration and transformation processes of pyrolysis volatile products of PL-NWCCL and FR4-NWPCB exhibit distinct patterns owing to the differences in substrates. Moreover, the pyrolysis pathways are intricate, encompassing depolymerization, chain scission, free–radical reactions, and secondary cracking or recombination.[2,26] The basic structure of PL-NWCCL and the reaction mechanism during its pyrolysis process are depicted in Fig. 12. As detailed in Section 3.3 of this paper, the chlorinated compounds of PL-NWCCL commence to form at 250 °C. At this temperature, Cl· radicals are preferentially released. Initially, they combine with CH_3· and subsequently with H·. When the pyrolysis temperature reaches 300°C the Br· radicals in TBBPA of PL-NWCCL start to dissociate. These radicals tend to first combine with CH_3· and then with H·,[67] resulting in the formation of CH_3Br and HBr, respectively. Chlorinated alkanes continue to decompose and react with C_2H_5·, C_3H_7·, C_4H_9·, and C_5H_{11}·, yielding C_2H_5Cl, C_3H_5Cl, C_3H_7Cl, C_4H_9Cl, and $C_5H_{11}Cl$. Subsequently, due to its relatively low bond energy (263 KJ mol^{-26}), the PhO–C bond between polymers breaks first. This is followed by chain-scission reactions of bonds such as Ph–C, C–C, and Ph–O, leading to the generation of C_3H_6O, epoxy resin monomers, *etc.* Additionally, through H–transfer processes, a diverse range of phenolic, ether, and ketone products are produced. Examples include phenol, p-cresol, p-isopropenylphenol,[68] along with C_8H_6O, C_2H_4O, *etc.* Simultaneously, the curing agent-DDS added to PL-WCCL also begins to decompose, generating C_3H_8S and C_6H_7N.

Particularly, the cellulose of the substrate in PL-NWCCL begins to decompose at 250 °C, forming $C_2H_4O_2$. During the pyrolysis process, cellulose also participates in the radical reaction of chlorine (Cl). It is likely that C_4H_7ClO is generated35, thereby exerting an inhibitory effect on the release of Cl· in the temperature range of 250–350 °C. As a result, above 500 °C, C_2H_5Cl, C_3H_5Cl, C_3H_7Cl, C_4H_9Cl, and $C_5H_{11}Cl$ are released in large quantities. Simultaneously, hydrocarbon compounds, ether compounds, and ketone compounds are further released.

The fundamental structure of FR4-NWPCB and the reaction mechanism underlying its pyrolysis process are illustrated in Fig. 13. Distinct from PL-NWCCL, the release of bromine and chlorine from halogen-based flame retardants remain unaffected. The primary When the pyrolysis temperature reaches 300 °C, Cl· and Br· radicals temperature range for their release is between 300 °C and 400 °C.[69] begin to be preferentially released. These radicals tend to first combine with CH_3· and subsequently with H·. Starting from the 8th minute of the isothermal stage at 300 °C, due to its relatively low bond energy (263 kJ mol^{-26}), the PhO–C linkage between polymers fractures first. Subsequently, other linkages such as Ph–C, C–C, and Ph–O

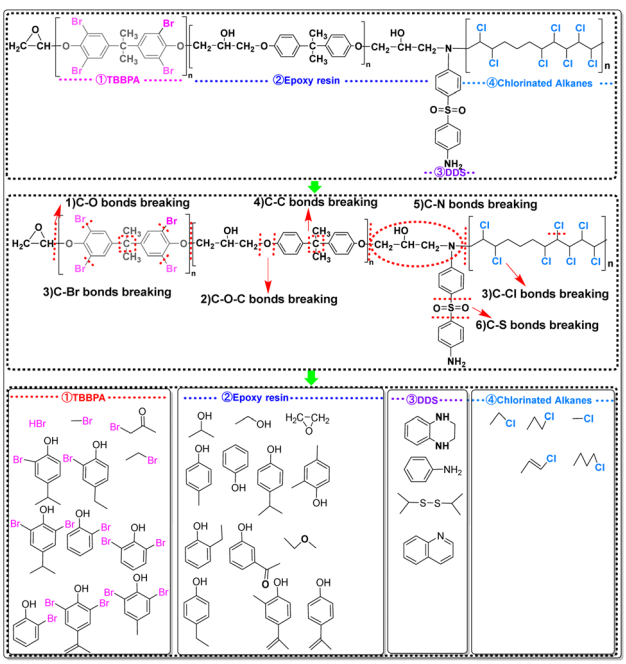

Fig. 12 Reaction mechanism of pyrolysis of PL-NWCCL.

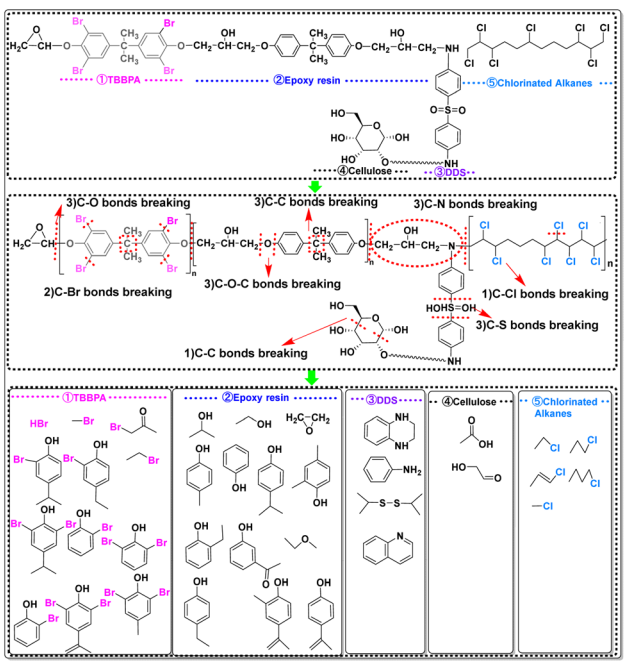

Fig. 13 Reaction mechanism of pyrolysis of FR4-NWPCB.

also undergo chain-scission reactions. Through hydrogen transfer processes, a diverse array of phenolic, ether, and ketone products are formed. Examples include phenol, p-cresol, p-isopropenylphenol,[68] along with C_8H_6O and C_2H_4O. Simultaneously, Cl· radicals continue to react with alkyl radicals, leading to the release of HCl, C_4H_9Cl and $C_5H_{11}Cl$. The added curing agent-DDS also commences decomposition during this period, producing C_3H_8S and C_6H_7N.

4 Conclusions

This study selected two representative waste printed circuit boards (WPCB) of different substrate as raw materials: copper-clad laminate scraps with wood pulp paper substrate (PL-WCCL) and waste printed circuit boards with glass fiber substrate (FR4-WPCB). Firstly, the proximate analysis and elemental analysis were conducted on them. The results showed that the C and the fixed carbon content of PL-WCCL accounted for 46.22% and 23.88% respectively, while the C and the fixed carbon content of FR4-WPCB was 37.7% and 2.74%. The Br and Cl contents were quantitatively analyzed by oxygen-nitrogen ion chromatography. The Br content of PL-WCCL was 21.962 mg g^{-1} and the Cl content was 21.154 mg g^{-1}; the Br content of FR4-WPCB was 43.743 mg g^{-1} and the Cl content was 8.477 mg g^{-1}. Subsequently, thermogravimetric (TG) analysis was employed to explore the pyrolysis characteristics of the two materials. The results indicated that the main weight-loss temperature of PL-NWCCL occurred in two stages: 233–330 °C and 470–520 °C. In contrast, for FR4-NWPCB, the main weight-loss temperature occurred in only one stage, from 292 °C to 422 °C.

In this research, an in-house designed online pyrolysis-mass spectrometry coupling apparatus was further employed to perform a dynamic and real-time monitoring of the entire process of pyrolysis volatile products of the two raw materials. The migration and transformation patterns of the pyrolysis volatile products of PL-NWCCL and FR4-NWPCB were thus derived. Evidently, notable differences exist between them, attributable to the distinct nature of the substrates.

(1) During the pyrolysis of PL-NWCCL, chlorinated compounds are released over a wide range of temperatures from 250 to 600 °C, mainly including HCl, CH_3Cl, C_2H_5Cl, C_3H_5Cl, C_3H_7Cl, C_4H_9Cl and $C_5H_{11}Cl$. During the pyrolysis process, the $Cl^{\bullet}$ radical tends to combine with CH_3· first to form CH_3Cl, then with C_2H_5·, C_3H_7· and H· to generate C_2H_5Cl, C_3H_7Cl and HCl, and then with C_3H_5· to produce C_3H_5Cl. As the pyrolysis temperature increases, the Cl· radical can also combine with C_4H_9· and C_5H_{11}· to form C_4H_9Cl and $C_5H_{11}Cl$. However, due to the inhibitory effect of cellulose, C_2H_5Cl, C_3H_7Cl, C_4H_9Cl, $C_5H_{11}Cl$ and HCl are not released in large quantities until 430 °C, and the release amount reaches the maximum at 530 °C and then gradually decreases. During the pyrolysis of FR4-NWPCB, the main release temperature of chlorinated compounds is between 300 and 400 °C, and they are basically completely released. The main chlorinated products include CH_3Cl, C_3H_7Cl, HCl, C_4H_9Cl and $C_5H_{11}Cl$. During the pyrolysis process, the Cl· radical tends to combine with CH_3· and C_3H_7· groups.

(2) During the pyrolysis of PL-NWCCL, the principal release temperature range of bromine-containing compounds is 285–600 °C. The major detectable products are HBr and CH_3Br. In the course of pyrolysis, the Br· radical preferentially combines with CH_3· to form CH_3Br. Subsequently, it combines with the H· radical to generate HBr. By 350 °C, the release is essentially complete, suggesting that the inhibitory effect of cellulose on Br is not prominent. During the pyrolysis of FR4-NWPCB, the main release temperature range of bromine-containing compounds is 300–400 °C, which is consistent with that of PL-NWCCL. The Br· adical also shows a tendency to preferentially combine with CH_3·.

(3) The phenolic compounds in the pyrolysis products of PL-NWCCL and the pyrolysis products of DDS are predominantly released in the temperature range of 300–450 °C. In contrast, hydrocarbon compounds, ether compounds, ketone compounds, and the pyrolysis products of cellulose exhibit secondary release events within the temperature interval of 430–600 °C. For FR4-NWPCB, the main release interval of phenolic compounds, hydrocarbon compounds, ether compounds, ketone compounds in its pyrolysis products, as well as the pyrolysis products of DDS, is concentrated between 300–400 °C.

Consequently, this study addresses the deficiencies in previous research regarding chlorinated flame retardants in WPCB during pyrolysis. It has been discovered that the cellulose in PL-WCCL exerts a "delaying" effect on the release of Br and Cl. Moreover, through the establishment of different isothermal holding periods during pyrolysis, the sequential release order of pyrolysis products has been determined. This further elucidates the pyrolysis reaction mechanism, providing a theoretical foundation for the dehalogenation research and recycling of WPCBs. Gaining a clear understanding of the release patterns and characteristics of pyrolysis products from these two representative type of WPCB is an essential prerequisite for implementing dehalogenation technologies that are "tailored to the materials", achieving a "circular economy", and ensuring the "optimal utilization of resources".

Author contributions

Meng Tian: conceptualization, methodology, investigation visualization, writing – original draft, data curation. Zihe Liu: data curation. Dongyin Ren: data curation, resources. Xianglan Zhang: conceptualization, writing – review editing, project administration, funding acquisition, supervision. Cai Tie: resources, software, writing – review editing.

Conflicts of interest

The authors declare that they have no known competing financial interests or personal relationships that could have appeared to influence the work reported in this paper.

Data availability

The data supporting this article have been included as part of the supplementary information (SI). Supplementary information is available. See DOI: https://doi.org/10.1039/d5ra06737e.

Acknowledgements

This work was supported by Guangdong Xingsheng Resource Recycling Co., Ltd (U0255).

References

1 M. Haghi, F. Fotovat and S. Yaghmaei, *Waste Manag.*, 2023, **17**, 532–544.
2 M. Li, P. M. N. J. Park and J. Song, *Int. J. Biol. Macromol.*, 2025, **331**, 143728.
3 Y.-M. Kim, T. U. Han, C. Watanabe, N. Teramae, Y.-K. Park and S. K. B. Hwang, *J. Anal. Appl. Pyrolysis*, 2015, **115**, 87–95.
4 M. P. Luda, A. I. Balabanovich, M. Zanetti and D. Guaratto, *Polym. Degrad. Stab.*, 2007, **92**, 1088–1100.
5 X. Zhu, Y. Ni, D. Wang, T. Zhang, S. Qu, F. Qiao, Y. Ren, C. Nie, X. Lyu, J. Qiu and L. Li, *J. Clean. Prod.*, 2020, **265**, 121840.
6 G. Grause, M. Furusawa, A. Okuwaki and T. Yoshioka, *Chemosphere*, 2008, **71**, 872–878.
7 I. Fayaz, G. M. Peerzada and N. B. Ganaie, *ACS Omega*, 2022, **7**, 1035–1047.
8 Y. Guida and H. Matsukami, *Env. Sci Technol*, 2023, **57**, 13136–13147.
9 The Global E - Waste Monitor, **https://www.itu.int/en/ITU-D/Environment/Pages/Publications/The-Global-E-waste-Monitor-2024.aspx**, accessed Mach 2024.
10 Y. Zhang, C. Zhou, Y. Liu, B. Yao, L. Chao, D. Fan, M. Yu, C. Liu and J. Dai, *Chem. Eng. J.*, 2025, **503**, 158377.
11 Z. Yao, M. Reinmöller, N. Ortuño, H. Zhou, M. Jin, J. Liu and R. Luque, *Prog. Energy Combust. Sci.*, 2023, **97**, 101086.
12 C. Ma, S. Kumagai, Y. Saito, T. Yoshioka, X. Huang, Y. Shao, J. Ran and L. Sun, *Environ. Sci. Technol.*, 2024, **58**, 1423–1440.
13 H. He, Y. Li, R. Shen, H. Shim, Y. Zeng, S. Zhao, Q. Lu, B. Mai and S. Wang, *Environ. Pollut.*, 2021, **290**, 118060.
14 C. Zhou, Y. Zhang, X. Xing, T. Zhang, A. A. Siyal, Y. Liu, J. Dai, J. Qu, C. Liu, B. Yao, L. Chao, L. Chen, Y. Chen, J. Wang, J. Dong and L. Wang, *J. Clean. Prod.*, 2023, **421**, 138546.
15 R. K. Nekouei, I. Tudela, F. Pahlevani and V. Sahajwalla, *Curr. Opin. Green Sustain. Chem.*, 2020, **24**, 14–20.
16 M. Altarawneh, A. Saeed, M. Al-Harahsheh and B. Z. Dlugogorski, *Prog. Energy Combust. Sci.*, 2019, **70**, 212–259.
17 Y. Zhang, C. Zhou, Y. Liu, T. Zhang, X. Li, L. Wang, J. Dai, J. Qu, C. Zhang, M. Yu, Y. Yuan, Y. Jin, H. Yu and J. Fu, *Energy*, 2022, **239**, 122383.
18 B. Debnath, S. Pati, S. Kayal, S. De and R. Chowdhury, *Environ. Sci. Pollut. Res.*, 2024, **31**, 42931–42947.
19 K. Huang, J. Zheng, W. Yuan, X. Wang, Q. Song, Y. Li, J. C. Crittenden, L. Wang and J. Wang, *Waste Manag.*, 2021, **124**, 8–16.
20 B. Zhang, S. Zhang, Z. Yang, W. Liu, B. Wu, M. Huang and B. Liu, *Compos. Part B Eng.*, 2024, **287**, 111803.
21 J. Wang, Z. Xi, R. Gao, B. Niu and Z. Xu, *Waste Manag.*, 2025, **191**, 191–202.
22 T. Zhang, X. Mao, J. Qu, Y. Liu, A. A. Siyal, W. Ao, J. Fu, J. Dai, Z. Jiang, Z. Deng, Y. Song, D. Wang and C. Polina, *J. Hazard. Mater.*, 2021, **402**, 123749.
23 J. Zhu, T. Huang, Z. Huang, B. Qin, Y. Tang, J. Ruan and Z. Xu, *J. Hazard. Mater.*, 2022, **421**, 126814.
24 X. T. Yin, M. Tian, M. Q. Liu and Y. Chen, *Tianjin Chem. Ind.*, 2022, **36**, 13–16.
25 W. Chen, Y. Chen, Y. Shu, Y. He and J. Wei, *J. Clean. Prod.*, 2021, **313**, 127881.
26 Y. Wu and B. Wang, *J. Energy Inst.*, 2025, **120**, 102080.
27 J. Liu, H. Wang, W. Zhang, T. Wang, M. Mei, S. Chen and J. Li, *J. Hazard. Mater.*, 2022, **431**, 128612.
28 J. J. Xiong, S. Q. Yu, D. D. Wu, X. S. Lü, J. H. Tang, W. H. Wu and Z. T. Yao, *Waste Manag. Res.*, 2020, **38**, 1251–1258.
29 Y. Zhou, W. Wu and K. Qiu, *Waste Manag.*, 2010, **30**, 2299–2304.
30 A. Shokri and F. Fotovat, *Thermochim. Acta*, 2023, **724**, 179513.
31 A. Thukral, A. V. Thulasiraman, A. K. Vuppaladadiyam, S. K. Patel, M. K. Jena, K. Shah, N. Gupta, R. Saha, A. Pal and P. Saini, *Circ. Econ.*, 2025, **4**, 100125.
32 M. Haghi, F. Fotovat, A. Shokri and S. Yaghmaei, *Process Saf. Environ. Prot.*, 2024, **188**, 735–748.
33 X. Huang, J. Ren, J.-Y. Ran, C.-L. Qin, Z.-Q. Yang and J.-P. Cao, *Fuel Process. Technol.*, 2022, **229**, 107175.
34 P. Bhattacharya, P. H. Steele, E. B. M. Hassan, B. Mitchell, L. Ingram and C. U. Pittman Jr., *Fuel*, 2009, **88**, 1251–1260.
35 J. Snow, J. Lederer, P. Kuráň and P. Koutník, *Fuel Process. Technol.*, 2023, **248**, 107823.
36 R. Gao, L. Zhan, J. Guo and Z. Xu, *J. Hazard. Mater.*, 2020, **383**, 121234.
37 R. Gao, B. Liu, L. Zhan, J. Guo, J. Zhang and Z. Xu, *J. Hazard. Mater.*, 2021, **403**, 123465.
38 R. Cao, R. Zhou, Y. Liu, D. Ma, J. Wang, Y. Guan, Q. Yao and M. Sun, *Waste Manag.*, 2022, **149**, 134–145.
39 X. Li, C. Nie, G. Li, Q. Gao, X. Li, S. Yan, L. Li, X. Zhu and X. Qin, *Sep. Purif. Technol.*, 2025, **359**, 130816.
40 Y. Noguchi, L. Zhang, T. Maruta, T. Yamane and N. Kiba, *Anal. Chim. Acta*, 2009, **640**, 106–109.
41 B. Boro and P. Tiwari, *Thermochim. Acta*, 2024, **736**, 179747.
42 F. Diaz, B. Flerus, S. Nagraj, K. Bokelmann, R. Stauber and B. Friedrich, *J. Sustain. Metall.*, 2018, **4**, 205–221.
43 W. Liu, J. Xu, J. Han, F. Jiao, W. Qin and Z. Li, *Chem. Eng.*, 2019, **7**, 1879–1889.
44 R. Gao and Z. Xu, *J. Hazard. Mater.*, 2019, **364**, 1–10.
45 A. I. Balabanovich, A. Hornung, D. Merz and H. Seifert, *Polym. Degrad. Stab.*, 2004, **85**, 713–723.
46 H.-H. Kim and B.-J. Kim, *Chem. Eng. J.*, 2024, **493**, 152407.
47 Q. Liu, X. Xu, L. Wang and D. Wang, *Chem. Eng. J.*, 2020, **400**, 125901.
48 R. Jin, M. Zheng, G. Lammel, B. A. M. Bandowe and G. Liu, *Energy Combust. Sci.*, 2020, **76**, 100803.
49 R. Jin, L. Yang, M. Zheng, Y. Xu, C. Li and G. Liu, *Environ. Pollut.*, 2018, **242**, 1346–1352.
50 Zs. Czégény, E. Jakab, M. Blazsó, T. Bhaskar and Y. Sakata, *J. Anal. Appl. Pyrolysis*, 2012, **96**, 69–77.
51 Y. Zhu, B. Li, Y. Wei, S. Zhou and H. Wang, *Process Saf. Environ. Prot.*, 2023, **178**, 1083–1093.
52 L. H. Perng, *J. Polym. Sci. Part Polym. Chem.*, 2000, **38**, 583–593.

53 S. Xie, C. Ma, S. Kumagai, Y. Takahashi, T. Kameda, Y. Saito and T. Yoshioka, *Sustain. Energy Fuels*, 2022, **6**, 1469–1478.
54 Z. Czégény, E. Jakab, J. Bozi and M. Blazsó, *J. Anal. Appl. Pyrolysis*, 2015, **113**, 123–132.
55 Y. Matsuzawa, M. Ayabe and J. Nishino, *Polym. Degrad. Stab.*, 2001, **71**, 435–444.
56 M. Altarawneh, O. H. Ahmed, M. Al-Harahsheh, Z.-T. Jiang, N. M. Huang, H. N. Lim and B. Z. Dlugogorski, *Chemosphere*, 2020, **254**, 126766.
57 J. Zhou, G. Liu, S. Wang, H. Zhang and F. Xu, *J. Energy Inst.*, 2020, **93**, 2362–2370.
58 D. Li, S. Lei, P. Wang, L. Zhong, W. Ma and G. Chen, *Renew. Energy*, 2021, **173**, 662–674.
59 R. Tien, T. Bernsmann, H.-U. Humpf and P. Fürst, *J. Agric. Food Chem.*, 2021, **69**, 7158–7167.
60 B. Yuan, T. Alsberg, C. Bogdal, M. MacLeod, U. Berger, W. Gao, Y. Wang and C. A. de Wit, *Anal. Chem.*, 2016, **88**, 8980–8988.
61 B. Yuan, D. H. Lysak, R. Soong, A. Haddad, A. Hisatsune, A. Moser, S. Golotvin, D. Argyropoulos, A. J. Simpson and D. C. G. Muir, *Environ. Sci. Technol. Lett.*, 2020, **7**, 496–503.
62 B. Yuan, C. Bogdal, U. Berger, M. MacLeod, W. A. Gebbink and T. Alsberg, *Environ. Sci. Technol.*, 2017, **51**, 10633–10641.
63 F. Zhang, Y. Wu, Q. Ye, J. Wang, Q. Wu, L. Zhou, W. Wu and S. Xie, *Environ. Res.*, 2025, **283**, 122101.
64 M. Yu, C. Zhang, X. Li, Y. Liu, A. A. Siyal, J. Qu, J. Dai, Y. Yuan, Y. Jin and C. Liu, *Fuel Process. Technol.*, 2023, **250**, 107898.
65 Y. Liu, C. Zhou, A. A. Siyal, C. Liu, Y. Zhang, J. Fu, H. Yun, J. Dai and X. Bi, *J. Clean. Prod.*, 2024, **437**, 140750.
66 Y. Zhu, B. Li, Y. Wei, S. Zhou and H. Wang, *Waste Manag.*, 2025, **193**, 84–94.
67 Y. Wu, R. Tao, B. Li, C. Hu, W. Zhang, H. Yuan, J. Gu and Y. Chen, *Sci. Total Environ.*, 2024, **912**, 169610.
68 A. Liu, Z. S. Zhao, G. B. Qu, Z. S. Shen, J. B. Shi and G. B. Jiang, *Environ. Pollut.*, 2018, **243**, 1141–1153.
69 J. Lu, H. Tu and G. Gu, *React. Funct. Polym.*, 2023, **193**, 105769.